Geosci. Model Dev. Discuss., 7, 4045–4079, 2014
www.geosci-model-dev-discuss.net/7/4045/2014/
doi:10.5194/gmdd-7-4045-2014

Geoscientific Model Development Discussions
Open Access

On the computation of planetary boundary layer height using the bulk Richardson number method

Y. Zhang[1,2], Z. Gao[1,2], D. Li[3,4], Y. Li[1], N. Zhang[5], X. Zhao[1], and J. Chen[1,6]

[1]International Center for Ecology, Meteorology & Environment, Jiangsu Key Laboratory of Agriculture Meteorology, Collaborative Innovation Center on Forecast and Evaluation of Meteorological Disasters, Nanjing University of Information Science and Technology, Nanjing 210044, China
[2]State Key Laboratory of Atmospheric Boundary Layer Physics and Atmospheric Chemistry (LAPC), Institute of Atmospheric Physics, Chinese Academy of Sciences, Beijing 100029, China
[3]Program of Atmospheric and Oceanic Sciences, Princeton University, Princeton, NJ 08540, USA
[4]NOAA/Geophysical Fluid Dynamics Laboratory, Princeton, NJ 08540, USA
[5]School of Atmospheric Sciences, Nanjing University, Nanjing, 210093, China
[6]Department of Geography, Michigan State University, East Lansing, MI 48824, USA

Received: 15 March 2014 – Accepted: 10 June 2014 – Published: 24 June 2014

Correspondence to: Z. Gao (zgao@mail.iap.ac.cn)

Published by Copernicus Publications on behalf of the European Geosciences Union.

GMDD
7, 4045–4079, 2014

Abstract

Experimental data from four intensive field campaigns are used to explore the variability of the critical bulk Richardson number, which is a key parameter for calculating the planetary boundary layer height (PBLH) in numerical weather and climate models with the bulk Richardson method. First, the PBLHs of three different thermally-stratified boundary layers (i.e., strongly stable boundary layer, weakly stable boundary layer, and unstable boundary layer) from the four field campaigns are determined using the turbulence method, the potential temperature gradient method, the low-level jet method, or the modified parcel method. Then for each type of boundary layer, an optimal critical Richardson numbers is obtained through linear fitting and statistical error minimization methods so that the bulk Richardson method with this optimal critical bulk Richardson number yields similar estimates of PBLHs as the methods mentioned above. We find that the optimal critical bulk Richardson number increases as the atmosphere becomes more unstable: 0.24 for strongly stable boundary layer, 0.31 for weakly stable boundary layer, and 0.39 for unstable boundary layer. Compared with previous schemes that use a single value of critical bulk Richardson number for calculating the PBLH, the new values of critical bulk Richardson number that proposed by this study yield more accurate estimate of PBLH.

1 Introduction

The planetary boundary layer (PBL) has significant impacts on weather, climate, and air quality (Stull, 1988; Garratt, 1992; Seidel et al., 2010). The height of the PBL (PBLH) is an important parameter that is commonly used in modeling atmospheric dispersion, turbulent mixing, convective transport, and cloud/aerosol entrainment (Deardorff, 1972; Holtslag and Nieuwstadt, 1986; Sugiyama and Nasstrom, 1999; Seibert et al., 2000; Medeiros et al., 2005; Konor et al., 2009; Liu and Liang, 2010; Leventidou et al., 2013).

GMDD
7, 4045–4079, 2014

The PBLH is usually viewed as the height where atmospheric turbulence diminishes upward from the surface (Stull, 1988). Using high-frequency data collected from ultrasonic anemometers on aircrafts, turbulence can be directly measured and the PBLH can be readily determined. This is known as the turbulence (Tur) method. It is highly reliable, but the instruments required by this method are costly. A more economic option to determine the PBLH is through analyzing temperature and wind profiles measured from radio soundings. In this study, the approaches that determine the PBLH from temperature and wind profiles are the focus. The atmospheric boundary layer is broadly classified as strongly stable boundary layer (Type I SBL), weakly stable boundary layer (Type II SBL), and unstable boundary layer (UBL) (Holtslag and Boville, 1993; Vogelezang and Holtslag, 1996). They are defined using the surface heat flux and the potential temperature profile, as shall be seen later.

For Type I SBL, turbulence is suppressed by negative buoyancy force. The PBLH is defined as the top of the inversion near the surface (Bradley et al., 1993), where the potential temperature gradient (PTG) first becomes smaller than a certain threshold (γ_s). $\gamma_s = 6.5\,\mathrm{K}\,(100\,\mathrm{m})^{-1}$ is used in this study following Dai et al. (2011). This is called the PTG method hereafter. For Type II SBL, turbulence is generated from wind shear due to relatively high wind speed and the PBLH is defined as the height of the low-level jet (LLJ) (Melgarejo and Deardorrff, 1974). This is called the LLJ method hereafter. For UBL, turbulence is generated from both shear and buoyancy and the PBLH is defined as the height at which a thin layer of capping inversion occurs. Under such conditions, the height at which a parcel of dry air, released adiabatically from the surface, reaches equilibrium with its environment is identified ("parcel method", Holzworth, 1964). This height is then corrected by another upward search for another height at which the potential temperature gradient first exceeds a threshold γ_c (Liu and Liang, 2010). In this study, $\gamma_c = 0.5\,\mathrm{K}\,(100\,\mathrm{m})^{-1}$ is used. This is called the modified parcel method hereafter.

For an atmosphere with discernible characteristics (i.e., a strongly stable profile for the Type I SBL, a strong LLJ for the Type II SBL, and a capping inversion layer for the UBL), the three methods generally show good performances (e.g., Mahrt et al., 1979;

GMDD
7, 4045–4079, 2014

Liu and Liang, 2010; Dai et al., 2011). However, for an atmosphere without discernible characteristics, large errors can be introduced by the methods, which limit their applications in numerical models. Instead, the bulk Richardson number (Ri_b) method is often used in numerical weather and climate models due to its reliability under a variety of atmospheric stability conditions (e.g., Holtslag and Boville, 1993; Jericevic and Grisogono, 2006; Richardson et al., 2013). The Ri_b method assumes that the PBLH is the height at which the Ri_b reaches its critical value (Ri_{bc}). The Ri_b at a certain height h is calculated with temperatures and wind speeds at this level and at the lower boundary of the PBL (generally the surface), following (Hanna, 1969):

$$Ri_b = \frac{(g/\theta_{v0})(\theta_{vh} - \theta_{v0})h}{u_h^2 + v_h^2}, \quad (1)$$

where θ_{v0} and θ_{vh} are the virtual potential temperatures at the surface and the height h, respectively; g/θ_{v0} is the buoyancy parameter, and u_h and v_h are the horizontal wind speed at the height h. The Ri_b method is also computationally cheap because it only requires low-frequency data. Nonetheless, a key parameter, the critical Richardson number (Ri_{bc}), has to be determined as a prior known. In previous studies, the value of Ri_{bc} varies in the range from 0.15 to 1.0 (Zilitinkevich and Baklanov, 2002; Jericevic and Grisogono, 2006; Esau and Zilitinkevich, 2010), with values of 0.25 and 0.5 most often used (e.g., Troen and Mahrt, 1986; Holtslag and Boville, 1993). One important reason for the large variation of Ri_{bc} is its dependence on the atmospheric stratification conditions. For example, Vogelezang and Holtslag (1996) reported the Ri_{bc} value of 0.16–0.22 in a nocturnal strongly stable condition and 0.23–0.32 in a weakly stable condition, while for the UBL, a value larger than 0.25 is usually needed (Zhang et al., 2011). Esau and Zilitinkevich (2010) also showed that Ri_{bc} was smaller for the nocturnal SBL than that for the conventionally neutral and long-lived stable PBL based on a large-eddy simulation database. Most recently, there is even a linear relationship between Ri_{bc} and atmospheric stability parameter has been proposed and examined (Richardson et al., 2013; Basu et al., 2014). This significant dependence of Ri_{bc} on

GMDD
7, 4045–4079, 2014

the atmospheric stability should be taken into account in the PBLH estimation, while in practice it is usually not considered.

The objective of this study is to determine the best choice of Ri_{bc} under different stratification conditions so that the estimate of PBLH with the Ri_b method is improved. The study is organized in the following way: Sect. 2 describes the data used in this study; Sect. 3 compares estimates of PBLH from different methods; Sect. 4 describes the best choices of Ri_{bc}, and Sect. 5 presents the conclusions.

2 Observational data

Observational data from four field campaigns that occur under different surface and atmospheric conditions are used in this study. These field campaigns are the Litang observation experiment, the Atmospheric Radiation Measurement (ARM) observation experiment, the surface heat budget of the arctic ocean experiment (SHEBA), and the cooperative atmosphere–surface exchange study (CASES) in 1999 (CASES99). Each of these four field campaigns are briefly described, as follows:

The Litang site is located in the southeast of the Tibetan Plateau, which is a plateau meadow. The campaign provides 105 effective radio soundings of wind and temperature in three observation periods (7–16 March, 13–22 May, and 7–16 July 2008), with a typical 6 h interval (about 00:30, 06:30, 12:30, and 18:30 LST). The 30 min mean wind and temperature at 3 m height collected by an eddy covariance system are also used for calculating Ri_b.

An ARM mobile facility deployment was carried out over a plain farmland in Shouxian, China, from 14 May to 28 December 2008. During the campaign, soundings were collected every 6 h (about 01:30, 07:30, 13:30, and 19:30 LST). Due to instrument malfunction, some data were eliminated and a total of 842 radio soundings remain. The 30 min averaged wind and temperature measured at 4 m height by an eddy covariance system are also used.

GMDD
7, 4045–4079, 2014

The ice station of SHEBA is located around the Canadian icebreaker December Groseilliers in the Arctic Ocean. The observation provides radio soundings from mid-October 1997 to early October 1998. During the experiment, rawinsondes were released 2–4 times a day (around 05:15, 11:15, 17:15, and 23:15 LST). Since the near-surface (2.5 m) data available from 29 October 1997 to 1 October 1998 at the SHEBA are hourly averages (Andreas et al., 1999; Persson et al., 2002), the surface observations and soundings do not overlap well in time. To ensure accuracy, only soundings that are within time difference less than 15 min from surface observations were used in this study, yielding a total of 168 records.

The CASES99 is the second experiment of CASES that took place in Kansas, USA. The terrain is relatively flat (average slopes = 0.5°) and lacks obstacles. The aircraft measurements in the campaign were accomplished by the National Oceanic and Atmospheric Administration (NOAA) Long-EZ and Wyoming King Air during 6–27 October 1999 when there was a stable atmosphere. The sampling frequencies were 25 Hz and 50 Hz, respectively. Due to the fact that the lowest flight level is restricted (e.g., for security reasons), only 35 effective aircraft soundings were used. The 5 min averaged near-surface (3 m) wind and temperature data were recorded at the NO.16 flux tower in CASES99 (www.eol.ucar.edu/projects/cases99). The surface observations and soundings in CASES99 overlap well in time, but their horizontal positions slightly differ from each other due to aircraft movement.

During the data processing, a 20 m moving-window average is used for all of the soundings from all of the sites (except the aircraft measurements in CASES99) to remove the measurement noise.

GMDD
7, 4045–4079, 2014

3 PBLH methods

3.1 The Tur, PTG, LLJ, and modified parcel methods that are used to determine PBLH from observational data

The PBL has a pronounced diurnal cycle (Stull, 1988; Garratt, 1992). It is typically shallow (< 500 m) at night, but grows deep (up to a few kilometers) during the day. As mentioned in the introduction, the PBL during a typical diurnal cycle can be categorized into three types: Type I SBL (i.e., strongly stable stratification at night), Type II SBL (i.e., weakly stable stratification at early morning/night), and UBL (i.e., unstable stratification during daytime). Based on previous studies (e.g., Holtslag and Boville, 1993; Vogelezang and Holtslag, 1996), the three types of atmospheric stratification can be separated using the surface heat flux H and the potential temperature θ profile:

$$\begin{cases} H \geq \delta & \text{for the UBL} \\ H < \delta \text{ and } \mathrm{d}^2\theta/\mathrm{d}z^2 < 0 & \text{for the Type I SBL} \\ \text{else} & \text{for the Type II SBL} \end{cases} \quad (2)$$

where $H = \rho C_p(\overline{w'\theta'})_0$ is the surface heat flux and θ is the potential temperature. δ is the minimum H for the unstable condition, which, in practice, is specified as small positive instead of zero (Liu and Liang, 2010). Due to different thermodynamic properties of land and ice, the value of δ is specified as $1\,\mathrm{W\,m^{-2}}$ over land and $0.5\,\mathrm{W\,m^{-2}}$ over ice through experimental verification. $\mathrm{d}^2\theta/\mathrm{d}z^2$ is calculated between 40 m and 200 m in this study; the selection of 40 m as the lower boundary is to avoid near-surface noises caused by landscape heterogeneity.

For any of the three types of atmospheric stratification, the Tur method is the most direct and accurate approach for the PBLH estimation because it measures the turbulence intensity directly. Figure 1 shows vertical profiles of potential temperature, wind speed, bulk Richardson number, and wind perturbations from CASES99 for the Type I (a1 to f1) and Type II SBL (a2 to f2). The perturbations (u', v', w'), which represent the

GMDD
7, 4045–4079, 2014

turbulence intensity, were obtained by removing the slowly varying part of the corresponding winds (u, v, w) through a high-pass wavelet filter (Wang et al., 1999; Wang and Wang, 2004). Then, using a continuous wavelet approach, the PBLH is detected as where a sharp drop of perturbations occurs with the maximum wavelet amplitude for all wavelet scales (Dai et al., 2011). The PBLHs determined by the Tur method are denoted by the red solid lines on Fig. 1d–f. It can be seen that with the PTG method (see the red solid line on a1) and the LLJ method (see the red solid line on b2), reasonable PBLHs can be obtained for Type I and II SBL, respectively, as compared to the Tur method.

Figure 2 further illustrates the sounding profiles and the PBLHs estimated by the PTG, LLJ, and modified parcel method for the three different boundary layers, respectively. The radio soundings were taken from Litang on 9 July 1997. At midnight (00:35 LST), the PBL was very stable due to radiative cooling from the surface. According to the PTG method, the PBLH was found at the top of the strong inversion (163 m, Fig. 2a). In early morning (06:35 LST), the surface temperature increased due to insolation and, thus, the inversion near the surface became weak; the low-level wind speed increased rapidly and formed a LLJ, while the vertical mixing caused by strong shear extended the inversion upward. With the LLJ method, the PBLH was determined at the height of the maximum wind (260 m, Fig. 2b). As the surface heating continues, a super-adiabatic layer (SAL), in which the potential temperature decreased with the height, formed near the surface and a UBL was developed by midday (12:45 LST). The vertical mixing caused by surface heating is limited by the presence of an inversion aloft. With the modified parcel method, the PBLH is determined to be 1754 m (Fig. 2c).

The three methods mentioned above are useful for an atmosphere boundary layer with discernible characteristics (Figs. 1 and 2). However, these methods may introduce large uncertainty under many other conditions (Fig. 3, and also see e.g., Russell et al., 1974; Martin et al., 1988; Balsley et al., 2006; Meillier et al., 2008). For the Type I SBL, when the underlying inversion is not strong, it will be difficult to determine the PBLH by the PTG method due to the fact that the maximum PTG can be less than

GMDD
7, 4045–4079, 2014

the threshold γ_s (Fig. 3a1–e1). For the Type II SBL, when there is no clear wind-speed maximum or when multiple maximums exist, the LLJ method will have difficulties in determining the PBLH. For example, there are two maximums in the wind profile at 160 m and 400 m, respectively (Fig. 3a2–e2). If the PBLH is simply determined as the lower height, it might result in an underestimation. Combining information from the Ri_b profile (Fig. 3c2), a more reasonable estimate of PBLH should be 400 m instead of 160 m. For the UBL, similar tricky situations can occur. The results of the modified parcel method with a specified PTG threshold may be subjective as the threshold generally depends on the vertical resolution and data precision (Beyrich, 1997; Joffre et al., 2001). For example, there are two PTG maximums at 900 m and 2000 m, respectively (Fig. 3a3–e3), which are consistent with the heights where the relative humidity sharply decreases. The PBLH is about 900 m when combining the information of the Ri_b profile (Fig. 3c3), while it might have been determined to be 2000 m by the modified parcel method if $\gamma_c = 0.5\,\mathrm{K}\,(100\,\mathrm{m})^{-1}$ is used.

Although these special cases do not always exist, they limit the applications of the three methods. The accuracy of the PBLH determination can be improved with additional information, as can be seen from Fig. 3. To sum up the procedures that are used in this study for estimating PBLH by using these three methods, first, for Type I SBL cases with a relatively weak underlying inversion (the local PTG maximum is $< 6.5\,\mathrm{K}\,(100\,\mathrm{m})^{-1}$ between 40–200 m), if there is a LLJ, the case is classified to a Type II SBL; if not, the PBLH is given as the first level of soundings above 40 m. Second, Type II SBL cases without clear wind-speed maximum are removed. Last, when there are multiple wind maximums for a Type II SBL or multiple PTG maximums for a UBL, the information from the Ri_b profile is combined to determine the PBLH. With these procedures, the obtained PBLHs by using these three methods are treated as "observed" PBLH hereafter.

GMDD
7, 4045–4079, 2014

3.2 The bulk Richardson number method

As mentioned in the introduction, the fundamental difference between the PBL and the atmosphere above the PBL (i.e., the free atmosphere) is the presence of turbulence in the PBL. The numerator and denominator of Eq. (1) represent the buoyancy destruction and the shear production of turbulent kinetic energy, respectively. Hence the Richardson number is an indicator of turbulence intensity (Stull, 1988) and, therefore, can be used to determine the PBLH.

To avoid overestimating the shear production in Eq. (1) for relatively high wind speeds (i.e., in Type II SBL) and to account for turbulence generated by surface friction under neutral conditions, Vogelezang and Holtslag (1996) proposed an updated model for calculating the Richardson number:

$$Ri_b = \frac{(g/\theta_{vs})(\theta_{vh} - \theta_{vs})(h - z_s)}{(u_h - u_s)^2 + (v_h - v_s)^2 + 100u_*^2}, \quad (3)$$

where z_s is the height of the lower boundary for the PBL (generally the top of the atmospheric surface layer), which is often taken as 20 m, 40 m, or 80 m for SBL (Vogelezang and Holtslag, 1996). For UBL, z_s is often taken as 0.1 PBLH (Troen and Mahrt, 1986) or the height of super-adiabatic layer (z_{SAL}) near the surface, as shall be seen later. Note for Eq. (1) the lower boundary for the PBL is chosen to be the surface while for Eq. (3) the lower boundary is not the surface. θ_{vs} is the virtual potential temperature at the height z_s, and u_s and v_s are the wind speed components at z_s. The term $100u_*^2$ makes Eq. (3) more applicable for the near-neutral condition, which is classified as a Type II SBL in this study (Seibert et al., 2000).

Under unstable conditions, the virtual potential temperature at the lower boundary θ_{vs} is replaced by θ'_{vs} (Troen and Mahrt, 1986; Holtslag et al., 1995):

$$\theta'_{vs} = \theta_{vs} + b_s \frac{\overline{(w'\theta'_v)_0}}{w_m}, \quad (4)$$

GMDD
7, 4045–4079, 2014

where $b_s = 8.5$, $(\overline{w'\theta'_v})_0$ is the virtual heat flux at the surface, and w_m is a turbulent velocity scale:

$$w_m = (u_*^3 + 0.6w_*^3)^{1/3}, \quad (5)$$

and

$$w_* = [\frac{g}{\theta_{v0}}(\overline{w'\theta'_v})_0 h]^{1/3} \quad (6)$$

is the convective velocity scale. The second term on the right hand side of Eq. (4) represents the temperature excess that is a measure of the strength of convective thermals.

Previous studies have shown that when using the Ri_b method, the choice of the lower boundary height z_s can significantly affect the PBLH estimation (Mahrt et al., 1981). Following Vogelezang and Holtslag (1996), the calculation is conducted with $z_s = 40$ m or 80 m but not with $z_s = 20$ m under stable conditions since $z_s = 20$ m is so close to the surface that results are strongly affected by the near-surface features. In the UBL, $z_s = 0.1$ PBLH or z_{SAL} for unstable conditions is used. z_{SAL} is identified as the height at which the potential temperature first reaches its minimum.

In this study, the virtual potential temperature is replaced by potential temperature in the calculation because the former can cause larger uncertainties due to inaccurate humidity measurements, which lead to significant fluctuations in the PBLH estimation (Liu and Liang, 2010).

After we estimate the Ri_b vertical profile from Eqs. (3–6), the PBLH can be obtained as the height where the Ri_b exceeds its critical value Ri_{bc}, which needs to be defined as a prior known (see Sect. 4).

GMDD
7, 4045–4079, 2014

4 Determination of the Ri_{bc}

In this study, the Ri_{bc} is retrieved as the Ri_b at the PBLH, which is determined by the PTG, LLJ, modified parcel methods with procedures described in Sect. 3.1 or by the Tur method. Because each profile provides a Ri_{bc} value, a representative Ri_{bc} at each experimental site for each stratification regime can be obtained. In Sect. 4.1, this is done by fitting a linear relationship between the numerator and the denominator of Eq. (3), and the slope of this linear relationship is viewed as a representative Ri_{bc}. In Sect. 4.2, a statistical error minimization method is used to retrieve a representative Ri_{bc}.

4.1 Representative Ri_{bc} from the linear fitting method

First, we determined the representative Ri_{bc} value for the Type I SBL (Fig. 4). The soundings are taken from Litang, CASES99, ARM, and SHEBA, with the height z_s of 40 m (left) and 80 m (right). Note that with $z_s = 80$ m, only cases with a PBLH ≥ 80 m are used. Except for CASES99, the fitted Ri_{bc} values of each site are about 0.25. The difference in Ri_{bc} for different z_s (40 or 80 m) is small. However, with $z_s = 40$ m, the results are slightly more consistent as compared to the results with $z_s = 80$ m, as can be seen from the higher correlation coefficient values at ARM and CASES99. The Ri_{bc} for the Type I SBL from CASES99 aircraft measurements is 0.20–0.21, which is slightly smaller than the value determined from radio soundings at other experimental sites. This may be due to the fact that the depth of the nocturnal inversion is generally thicker than the depth of the turbulent layer (Mahrt et al., 1979; Andre and Mahrt, 1982). Therefore, the PBLH determined by the Tur method is smaller than that determined by the PTG method. Note the Tur method is used to determine the PBLH for CASES99 but the PTG method is used for the other three campaigns.

The linear fittings between the numerator and denominator of Eq. (3) for the Type II SBL soundings are shown in Fig. 5. Compared to the results in Fig. 4, the correlation coefficients in Fig. 5 are smaller, indicating that the PBLH is more difficult to determine

GMDD
7, 4045–4079, 2014

for weakly stable boundary layers (Esau and Zilitinkevich, 2010). The correlation coefficients indicate that the agreement at $z_s = 80$ m is slightly better than at $z_s = 40$ m. In particular, the Ri_{bc} is sensitive to the height z_s in the SHEBA data. It changes from 0.21 to 0.29 as the height z_s changes from 40 m to 80 m. The main cause of the large deviation is because the LLJ above the ice surface in SHEBA is considerably strong (up to 20 m s^{-1}) and the vertical wind speed gradient is large, so the denominator in Eq. (3) decreases more rapidly with the height z_s than the numerator, which leads to an increase in the Ri_{bc} value. On the other hand, the Ri_{bc} over land from Litang and ARM ranges from 0.25 to 0.27 and hence varies little with z_s (Fig. 5), which is consistent with the findings of Vogelezang and Holtslag (1996) using Cabauw mast data and SODAR data.

For the UBL, the height z_s was given as 0.1PBLH (left) and z_{SAL} (right) (Fig. 6). The scatter diagram shows that the correlation coefficients are smaller than 0.4 at all sites, implying large variability in the Ri_{bc} from each UBL sounding. The representative value of Ri_{bc} is larger than 0.25 and varies from 0.28 to 0.34. However, it appears that the PBLH estimated by the bulk Richardson number method seems to be insensitive to a particular value of Ri_{bc}. The estimates of PBLH from the Ri_b method with $Ri_{bc} = 0.25$ or 0.5 are both in good agreement with the estimates from the modified parcel method at the three sites (Fig. 7). This is consistent with some previous studies (Troen and Mahrt, 1986). Therefore, the Ri_b method can still be used to reliably estimate the PBLH under such conditions, despite that the Ri_{bc} retrieved using the linear fitting method shows a large variability. In the next section, several statistical error minimization methods are used to retrieve a representative Ri_{bc} value under unstable conditions.

4.2 Representative Ri_{bc} from the error minimization method

It is seen that the linear fitting method is not applicable for retrieving an optimal value of the Ri_{bc} under unstable conditions due to the small correlation coefficients. Under stable conditions, the linear fitting method also has some disadvantages. For example,

GMDD
7, 4045–4079, 2014

the fitted value of the Ri_{bc} and the correlation coefficient highly depend on the larger value points, while the impact of the smaller value points is reduced (Fig. 4a2). Therefore, error minimization methods are used in this section to determine a representative Ri_{bc}. The values of Ri_{bc} between 0.1–0.4 in stable conditions and 0.2–0.5 in unstable conditions are first used to calculate the PBLH; then, three statistical variables are used to examine the accuracy of the estimated PBLH (Gao et al., 2004):

$$\text{Bias} = \frac{\sum_{i=1}^{n} \left| h_{Ri_b} - h_{obs} \right|}{n}, \tag{7}$$

$$\text{SEE} = \sqrt{\frac{\sum_{i=1}^{n} \left| h_{Ri_b} - h_{obs} \right|^2}{n-2}}, \tag{8}$$

$$\text{NSEE} = \sqrt{\frac{\sum_{i=1}^{n} \left(h_{Ri_b} - h_{obs} \right)^2}{\sum_{i=1}^{n} (h_{obs})^2}}, \tag{9}$$

where h_{Ri_b} is the estimated value by the Ri_b method, and h_{obs} represents the observed PBLH (i.e., calculated using the Tur, PTG, LLJ, or modified parcel method). Bias, SEE, and NSEE are the bias, standard error, and normalized standard error of h_{Ri_b} against h_{obs}, respectively, and n is the sampling number. Optimal values of Ri_{bc} can be determined based on the minimum Bias, SEE, and NSEE. However, the optimal Ri_{bc} determined based on the minimum Bias, or minimum SEE and NSEE can be different (note that minimum SEE and NSEE yield the same optimal Ri_{bc}). In this study, the optimal Ri_{bc} values retrieved from minimum SEE and NSEE are treated as the best because the bias cannot reflect the dispersion of data. To compare the linear fitting method and

GMDD
7, 4045–4079, 2014

the error minimization method, the correlation coefficients determined using the linear fitting method (see Figs. 4 to 6) are also presented.

The correlation coefficient, Bias, SEE, and NSEE calculated with different values of Ri_{bc} under the Type I SBL are shown in Fig. 8. These scattered data are fitted with quadratic curves and then the maximum or minimum of the curves can be obtained, which are used to select the optimal Ri_{bc} for each site. The weighted averages based on the sampling number at the four sites are used as the representative optimal Ri_{bc} for this stratification condition (see the black dashed lines in Fig. 8). The error bars depict the range of the optimal Ri_{bc} across the four sites (Fig. 8). The different optimal Ri_{bc} values from different sites are probably caused by the influences of surface conditions (e.g., surface roughness). By comparing the results with z_s = 40 m and 80 m, it can be seen that the error bars are smaller with z_s = 40 m and thus the optimal Ri_{bc} across different sites is more consistent with z_s = 40 m. Furthermore, the maximum correlation coefficient is larger and the minimum Bias, SEE, and NSEE are smaller with z_s = 40 m.

Compared to the Type I SBL, the correlation coefficient is smaller and the errors are larger for the Type II SBL (Fig. 9), again indicating that it is more difficult to determine the PBLH for weakly stable boundary layers. However, the maximum correlation coefficient, minimum Bias, minimum SEE and NSEE, and the range of optimal Ri_{bc} show smaller differences between different z_s (40 or 80 m). Compared to the results with the linear fitting method, the values of Ri_{bc} are generally larger for each site, which is understandable given that the scatter are mostly above the fitted lines in Fig. 5, especially in ARM and SHEBA. The optimal Ri_{bc} from minimum SEE and NSEE for the Type II SBL are 0.30–0.31. These results are consistent with the value (= 0.3) from Melgarejo and Deardorff (1974).

For unstable boundary layer (Fig. 10), the maximum correlation coefficient is larger, the minimum Bias, SEE, and NSEE are smaller, and the values of optimal Ri_{bc} are more concentrated with $z_s = z_{SAL}$ (bottom panels) as compared to z_s = 0.1 PBLH (top panels). Therefore, using z_{SAL} as the lower boundary height is more appropriate to estimate the UBL height. The minimum SEE and NSEE indicate that the optimal

GMDD
7, 4045–4079, 2014

Ri_{bc} = 0.39. The results with z_s = 40 or 80 m are also examined, which shows that the maximum correlation coefficient and minimum Bias, SEE, and NSEE are close to those with z_s = 0.1 PBLH, but the values of optimal Ri_{bc} are more scattered across different sites.

Through the above statistical error minimization methods, the optimal Ri_{bc} at different sites for the three stratification regimes and with different choice of z_s are obtained (Table. 1). It appears that the optimal Ri_{bc} value increases when the stability of the stratification decreases. For the Type I SBL, the optimal Ri_{bc} value is 0.24 (z_s = 40 m) and 0.23 (z_s = 80 m); for the Type II SBL, the optimal Ri_{bc} value is 0.30 (z_s = 40 m) and 0.31 (z_s = 80 m); and for the UBL, the optimal Ri_{bc} value falls between 0.33 and 0.39, depending on the choice of z_s. In short, the best choices of Ri_{bc} suggested by this study are 0.24 (z_s = 40 m), 0.31 (z_s = 80 m), and 0.39 ($z_s = z_{SAL}$) for the Type I SBL, Type II SBL, and UBL, respectively. Note the height z_s is chosen as 80 m for Type II SBL, given that the surface layer is usually thicker for Type II SBL than for Type I SBL.

4.3 Impacts of thermal stratification on Ri_{bc}

With the above analyses, the best choices of Ri_{bc} are identified under different atmospheric stratification conditions. However, the PBLH is traditionally determined by the Ri_b method using a single value of Ri_{bc} without considering the dependence of Ri_{bc} on thermal stratification (e.g., Troen and Mahrt, 1986). For example, the Weather Research and Forecasting (WRF) model's YSU scheme assumes Ri_{bc} = 0.25 over land, while Ri_{bc} = 0.5 is used in the Holtslag and Boville (HB) boundary-layer scheme of the NCAR Community Climate Model version 2 (CCM2). To examine the impacts of different stratification conditions on Ri_{bc}, we obtained a single representative Ri_{bc} for all stratification conditions with the same sounding data (Litang, ARM, SHEBA), assuming the lower boundary height z_s of 40 m, 80 m, and z_{SAL} for the Type I SBL, Type II SBL, and UBL, respectively (Fig. 11). According to the minimum SEE and NSEE, the optimal choice of Ri_{bc} for all PBL types is 0.33, which is close to that used in the NCAR Community Atmosphere Model version 4 (CAM4, Ri_{bc} = 0.3).

GMDD
7, 4045–4079, 2014

Errors in model-predicted quantities will in turn lead to errors in the parameterized PBLH in full-model online evaluation (Liu et al., 2013), suggesting a need for direct offline evaluation. In the offline test, the PBLHs are calculated by different schemes with the same soundings and lower boundary heights. The new scheme uses Ri_{bc} = 0.24, 0.31, and 0.39 for the Type I SBL, Type II SBL, and UBL, respectively; while the other three schemes use a constant Ri_{bc} for all thermally-stratified conditions (Ri_{bc} = 0.33, Ri_{bc} = 0.25 in WRF-YSU, and Ri_{bc} = 0.5 in CCM2-HB). The results of these schemes are compared with the PBLH observation. We found that the new scheme with the Ri_{bc} identified in this study is more reliable in estimating PBLH (Fig. 12), which indicates that the impacts of stability on Ri_{bc} are significant in the PBLH parameterization with the Ri_b method. The only exception is that at SHEBA the new scheme and the other schemes show small differences. This may be resulted from the characteristics of the surface at this ice site and the weak diurnal cycle of stability.

5 Conclusions

The PBLH is an important length scale in atmospheric models. Accurate estimation of the PBLH is vital for the reliability of model simulation results. We investigated several methods for the PBLH under different stratification conditions. The Tur method is considered as the most accurate approach for any atmospheric stratification due to its direct measurement of turbulence strength. However, such a technique is expensive and cannot be widely applied. On the other hand, determination of the PBLH with radio soundings through the PTG, LLJ, and modified parcel methods is more affordable. However, these methods are not applicable in numerical models because they may fail to identify the PBLH under special conditions (e.g., a weak underlying inversion for the Type I SBL, multiple wind maximums for the Type II SBL, and no clear maximum of vertical gradient of potential temperature for the UBL). With corrections made for these special cases, we used the PTG, LLJ, and modified parcel methods to determine PBLHs from the radio soundings from Litang, ARM Shouxian, SHEBA, and

GMDD
7, 4045–4079, 2014

CASES99 field experiments and the estimated PBLH from these methods are treated as PBLH observations.

The Ri_b method is commonly used in numerical models due to its reliability for all atmospheric stratification conditions. In many numerical models, the Ri_{bc} is always specified as one single value (e.g., 0.25 for WRF-YSU scheme, 0.5 for CCM2-HB scheme) and hence its dependence on the atmospheric stratification conditions is ignored. This study identifies the Ri_{bc} for each stratification condition with PBLH observations through linear fitting and statistical error minimization approaches. The minimum SEE and NSEE indicate that the best choices for Ri_{bc} are 0.24, 0.31, and 0.39 for the Type I SBL, Type II SBL, and UBL, respectively. Compared with the single $Ri_{bc} = 0.33$ for all stratification conditions as well as $Ri_{bc} = 0.25$ and 0.5 that are currently used in WRF-YSU and CCM2-HB, respectively, the new Ri_{bc} values determined in this study yield more reliable PBLH estimations, suggesting that the variation of Ri_{bc} should be considered in the PBLH parameterization. Therefore, it is expected that the new Ri_{bc} values, when used in numerical models, will help to improve model results.

Acknowledgements. This study is supported by the China Meteorological Administration under grant GYHY201006024, the National Program on Key Basic Research Project of China (973) under grants 2012CB417203 and 2011CB403501, the National Natural Science Foundation of China under grant 41275022, and the CAS Strategic Priority Research Program, grant 5 XDA05110101.

References

Andre, J. C. and Mahrt, L.: The nocturnal surface inversion and influence of clear-air radiative cooling, J. Atmos. Sci., 39, 864–878, 1982.

Andreas, E. L., Fairall, C. W., Guest, P. S., and Persson, P. O. G.: An overview of the SHEBA atmospheric surface flux program, in: Preprints, Fifth Conference On Polar Meteorology and Oceanography, 10–15 January 1999, Dallas, Tex., American Meteorological Society, Boston, 411–416, 1999.

GMDD
7, 4045–4079, 2014

Balsley, B. B., Frehlich, R. G., Jensen, M. L., and Meillier, Y.: High-resolution in situ profiling through the stable boundary layer: examination of the SBL top in terms of minimum shear, maximum stratification, and turbulence decrease, J. Atmos. Sci., 63, 1291–1307, 2006.
Basu, S., Holtslag, A. A. M., Caporaso, L., Riccio, A., and Steeneveld, G. J.: Observational support for the stability dependence of the bulk Richardson number across the stable boundary layer, Bound.-Lay. Meteorol., 150, 515–523, doi:10.1007/s10546-013-9878-y, 2014.
Beyrich, F.: Mixing height estimation from sodar data-a critical discussion, Atmos. Environ., 31, 3941–3954, 1997.
Bradley, R. S., Keimig, F. T., and Diaz, H. F.: Recent changes in the North American Arctic boundary layer in winter, J. Geophys. Res., 98, 8851–8858, doi:10.1029/93JD00311, 1993.
Dai, C. Y., Gao, Z. Q., Wang, Q., and Cheng, G.: Analysis of atmospheric boundary layer height characteristics over the Arctic Ocean using the aircraft and GPS soundings, Atmos. Oceanic Sci. Lett., 4, 124–130, 2011.
Deardorff, J. W.: Parameterization of the planetary boundary layer for use in general circulation models, Mon. Weather Rev., 100, 93–106, 1972.
Esau, I. and Zilitinkevich, S.: On the role of the planetary boundary layer depth in the climate system, Adv. Sci. Res., 4, 63–69, doi:10.5194/asr-4-63-2010, 2010.
Gao, Z., Chae, N., Kim, J., Hong, J., Choi, T., Lee, H.: Modeling of surface energy partitioning, surface temperature, and soil wetness in the Tibetan prairie using the Simple Biosphere Model 2 (SiB2), J. Geophys. Res., 109, D06102, doi:10.1029/2003JD004089, 2004.
Garratt, J. R.: The Atmospheric Boundary Layer, Cambridge University Press, 316 pp., 1992.
Hanna, S. R.: The thickness of the planetary boundary layer, Atmos. Environ., 3, 519–536, 1969.
Holtslag, A. A. M. and Boville, B. A.: Local versus nonlocal boundary-layer diffusion in a global climate model, J. Climate, 6, 1825–1842, 1993.
Holtslag, A. A. M. and Nieuwstadt, F. T. M.: Scaling the atmospheric boundary layer, Bound.-Lay. Meteorol., 36, 201–209, 1986.
Holtslag, A. A. M., van Meijgaard, E., and de Rooy, W. C.: A comparison of boundary layer diffusion schemes in unstable conditions over land, Bound.-Lay. Meteorol., 76, 69–95, 1995.
Holzworth, C. G.: Estimates of mean maximum mixing depths in the contiguous United States, Mon. Weather Rev., 92, 235–242, 1964.
Jericevic, A. and Grisogono, B.: The critical bulk Richardson number in urban areas: verification and application in a numerical weather prediction model, Tellus A, 58, 19–27, 2006.

GMDD
7, 4045–4079, 2014

Joffre, S. M., Kangas, M., Heikinheimo, M., and Kitaigorodskii, S. A.: Variability of the stable and unstable atmospheric boundary-layer height and its scales over a boreal forest, Bound.-Lay. Meteorol., 99, 429–450, 2001.
Konor, C. S., Boezio, G. C., Mechoso, C. R., and Arakawa, A.: Parameterization of PBL processes in an atmospheric general circulation model: description and preliminary assessment, Mon. Weather Rev., 137, 1061–1082, 2009.
Leventidou, E., Zanis, P., Balis, D., Giannakaki, E., Pytharoulis, I., and Amiridis, V.: Factors affecting the comparisons of planetary boundary layer height retrievals from CALIPSO, ECMWF and radiosondes over Thessaloniki, Greece, Atmos. Environ., 74, 360–366, 2013.
Liu, G., Liu, Y., Endo, S.: Evaluation of surface flux parameterizations with long-term ARM observations, Mon. Weather Rev., 141, 773–797, 2013.
Liu, S. and Liang, X. Z.: Observed diurnal cycle climatology of planetary boundary layer height, J. Climate, 23, 5790–5809, doi:10.1175/2010JCLI3552.1, 2010.
Mahrt, L.: Modelling the depth of the stable boundary layer, Bound.-Lay. Meteorol., 21, 3–19, 1981.
Mahrt, L., Heald, R. C., Lenschow, D. H., Stankov, B. B., and Troen, I.: An observational study of the nocturnal boundary layer, Bound.-Lay. Meteorol., 17, 247–264, 1979.
Martin, C. L., Fitzjarrald, D., Garstang, M., Oliveira, A. P., Greco, S., and Browell, E.: Structure and growth of the mixing layer over the Amazonian rain forest, J. Geophys. Res., 93, 1361–1375, 1988.
Medeiros, B., Hall, A., and Stevens, B.: What controls the climatological depth of the PBL?, J. Climate, 18, 2877–2892, doi:10.1175/JCLI3417.1, 2005.
Meillier, Y. P., Froehlich, R. G., Jones, R. M., and Balsley, B. B.: Modulation of small-scale turbulence by ducted gravity waves in the nocturnal boundary layer, J. Atmos. Sci., 65, 1414–1427, 2008.
Melgarejo, J. W. and Deardorff, J.: Stability functions for the boundary-layer resistance laws based upon observed boundary-layer heights, J. Atmos. Sci., 31, 1324–1333, 1974.
Persson, P. O. G., Fairall, C. W., Andreas, E. L., Guest, P. S., and Perovich, D. K.: Measurements near the atmospheric surface flux group tower at SHEBA: near-surface conditions and surface energy budget, J. Geophys. Res., 107, 8045, doi:10.1029/2000JC000705, 2002.
Richardson, H., Basu, S., and Holtslag, A. A. M.: Improving stable boundary-layer height estimation using a stability-dependent critical bulk Richardson number, Bound.-Lay. Meteorol., 148, 93–109, doi:10.1007/s10546-013-9812-3, 2013.

GMDD
7, 4045–4079, 2014

Russell, P. B., Uthe, E. E., Ludwig, F. L., and Shaw, N. A.: A comparison of atmospheric structure as observed with monostatic acoustic sounder and lidar techniques, J. Geophys. Res., 79, 5555–5566, 1974.
Seibert, P., Beyrich, F., Gryning, S. E., Joffre, S., Rasmussen, A., and Tercier, P.: Review and intercomparison of operational methods for the determination of the mixing height, Atmos. Environ., 34, 1001–1027, 2000.
Seidel, D. J., Ao, C. O., and Li, K.: Estimating climatological planetary boundary layer heights from radiosonde observations: comparison of methods and uncertainty analysis, J. Geophys. Res., 115, D16113, doi:10.1029/2009JD013680, 2010.
Stull, R. B.: An Introduction to Boundary Layer Meteorology, Kluwer Academic, 666 pp., 1988.
Sugiyama, G. and Nasstrom, J. S.: Methods for Determining the Height of the Atmospheric Boundary Layer, UCRL-ID-133200, Lawrence Livermore National Laboratory Report, 1999.
Troen, I. and Mahrt, L.: A simple model of the planetary boundary layer: sensitivity to surface evaporation, Bound.-Lay. Meteorol., 37, 129–148, 1986.
Vogelezang, D. H. P. and Holtslag, A. A. M.: Evaluation and model impacts of alternative boundary-layer height formulations, Bound.-Lay. Meteorol., 81, 245–269, doi:10.1007/BF02430331, 1996.
Wang, Q. and Wang, S.: Turbulent and thermodynamic structure of the autumnal arctic boundary layer due to embedded clouds, Bound.-Lay. Meteorol., 113, 225–247, 2004.
Wang, Q., Lenschow, D. H., Pan, L., Schillawski, R. D., Kok, G. L., Prevot, A. S. H., Laursen, K., Russell, L. M., Bandy, A. R., Thornton, D. C., Suhre, K.: Characteristics of the marine boundary layers during two Lagrangian measurement periods: 2. Turbulence structure, J. Geophys. Res., 104, 21767–21784, 1999.
Zilitinkevich, S. S. and Baklanov, A.: Calculation of the height of stable boundary layers in practical applications, Bound.-Lay. Meteorol., 105, 389–409, 2002.
Zhang, J. A., Rogers, R. F., Nolan, D. S., and Marks, F. D.: On the characteristic height scales of the hurricane boundary layer, Mon. Weather Rev., 139, 2523–2535, 2011.

GMDD
7, 4045–4079, 2014

Table 1. Retrieved critical bulk Richardson number, Ri_{bc}, for different boundary layer regimes and sites, with different values of z_s. nr refers to the sample number.

Regime	z_s (m)	Litang		CASES99		ARM		SHEBA		Total	
		Ri_b	nr	Ri_b	nr	Ri_b	nr	Ri_b	nr	Ri_b	nr
Type I	40	0.25	21	0.22	29	0.24	400	0.25	27	0.24*	477
	80	0.26	11	0.21	21	0.23	211	0.24	17	0.23	261
Type II	40	0.27	53	\		0.32	194	0.24	49	0.30	296
	80	0.24	53	\		0.33	194	0.31	49	0.31*	296
UBL	40	0.41	23	\		0.36	182	0.20	75	0.33	280
	80	0.41	23	\		0.38	182	0.32	75	0.39	280
	0.1PBLH	0.42	23	\		0.39	182	0.34	62	0.38	267
	z_{SAL}	0.39	23	\		0.41	182	0.36	75	0.39*	280

* indicates the best choice.

GMDD
7, 4045–4079, 2014

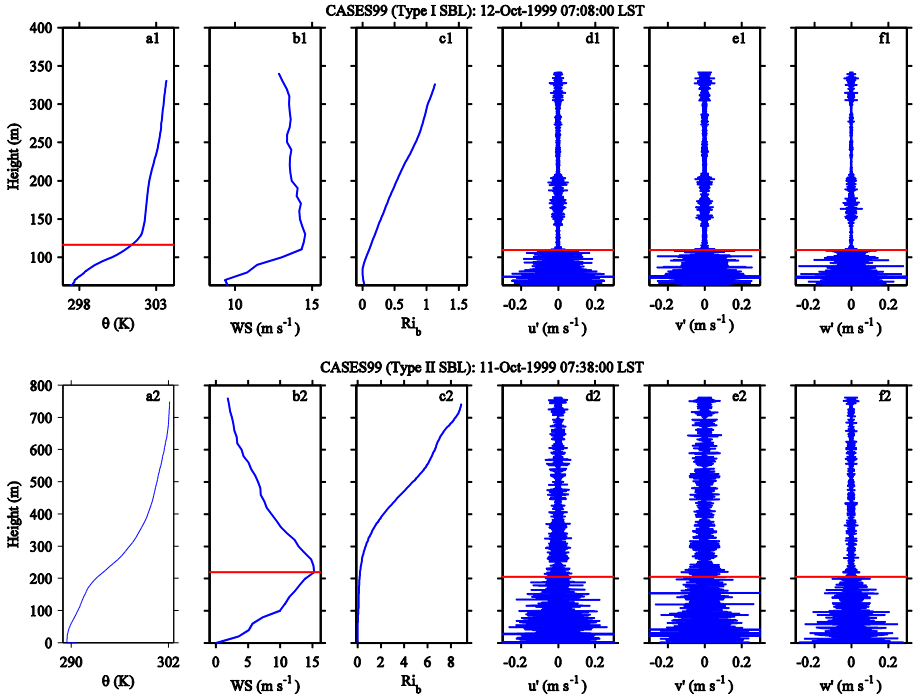

Figure 1. Examples of the vertical profiles of the Type I SBL (upper panels) and the Type II SBL (lower panels) from CASES99 aircraft measurements: **(a)** potential temperature (K); **(b)** horizontal wind speed ($m\,s^{-1}$); **(c)** bulk Richardson number Ri_b; **(d)** u perturbation ($m\,s^{-1}$); **(e)** v perturbation ($m\,s^{-1}$); **(f)** w perturbation ($m\,s^{-1}$). The red solid lines on (**a1** and **b2**) denote the PBLH calculated by the PTG and LLJ methods, respectively, and those on **(d–f)** denote the PBLH determined by the Tur method.

GMDD
7, 4045–4079, 2014

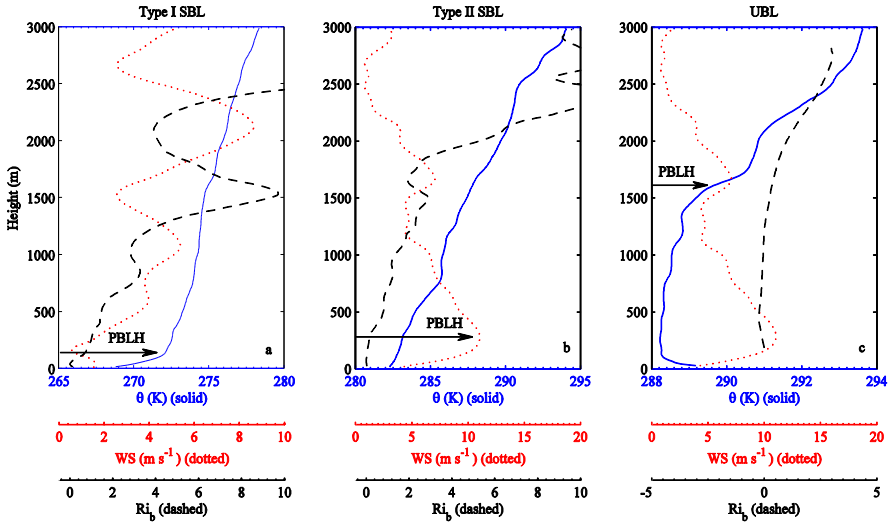

Figure 2. Typical profiles of potential temperature (blue), wind speed (red), and Ri_b (black) for different types of boundary-layers: **(a)** Type I SBL, **(b)** Type II SBL, and **(c)** UBL. The indicated PBLHs in **(a–c)** are calculated by the PTG, LLJ, and modified parcel methods, respectively. The observations in **(a–c)** are from Litang on 8 July 2008 16:35 UTC (00:35 LST), 8 July 2008 22:45 UTC (06:45 LST), and 9 July 2008 04:45 UTC (12:45 LST), respectively.

GMDD
7, 4045–4079, 2014

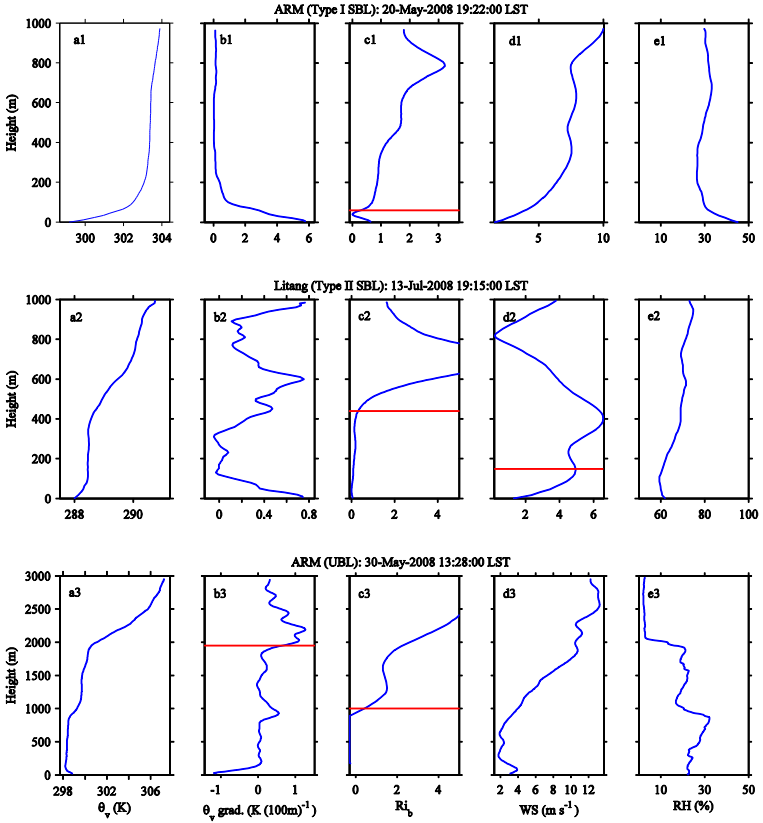

Figure 3. Examples of vertical profiles of the Type I SBL (upper panels), Type II SBL (middle panels), and UBL (lower panels): **(a)** potential temperature (K); **(b)** vertical gradient of potential temperature (K (100 m)$^{-1}$); **(c)** bulk Richardson number Ri_b; **(d)** horizontal wind speed (m s^{-1}); **(e)** relative humidity (%). The red solid lines on (**c1–c3, d2** and **b3**) denote the PBLH determined by the Ri_b, LLJ, and modified parcel methods, respectively.

GMDD
7, 4045–4079, 2014

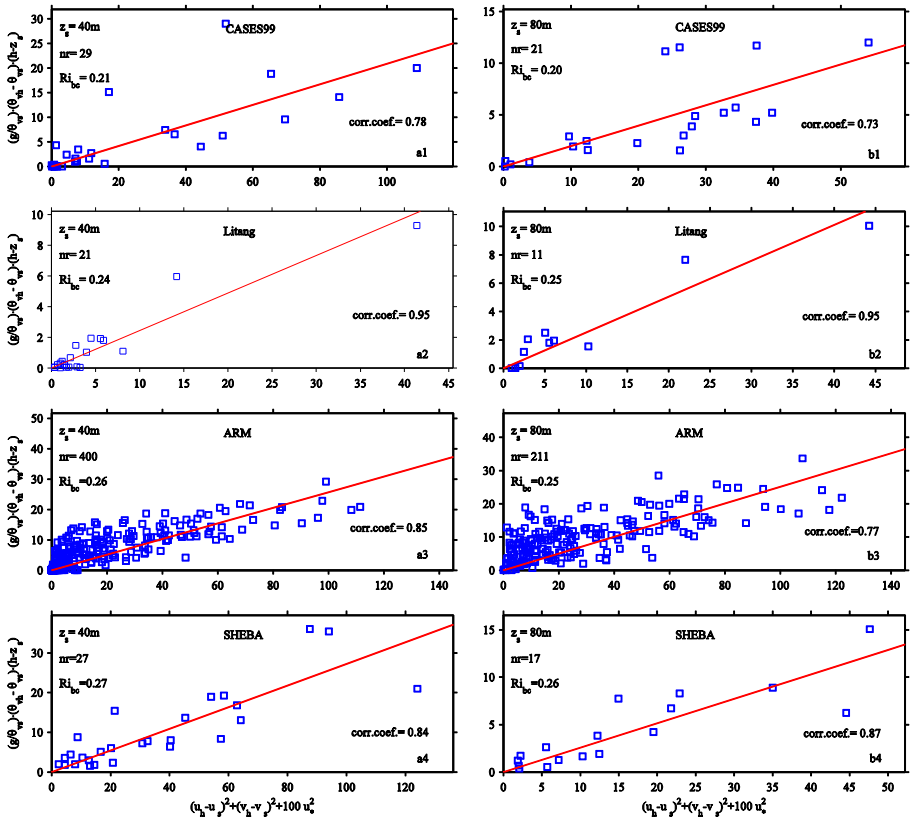

Figure 4. Comparisons of the numerator and denominator from Eq. (3) for the Type I SBL, with z_s at 40 m (left) and 80 m (right). The PBLHs determined by the PTG method for Litang, ARM Shouxian, and SHEBA data and by the Tur method for CASES99 data are used. nr refers to the effective sample number. The red solid lines are the best linear fittings of the data from different sites and their slopes represent the values of the critical bulk Richardson number Ri_{bc}.

GMDD
7, 4045–4079, 2014

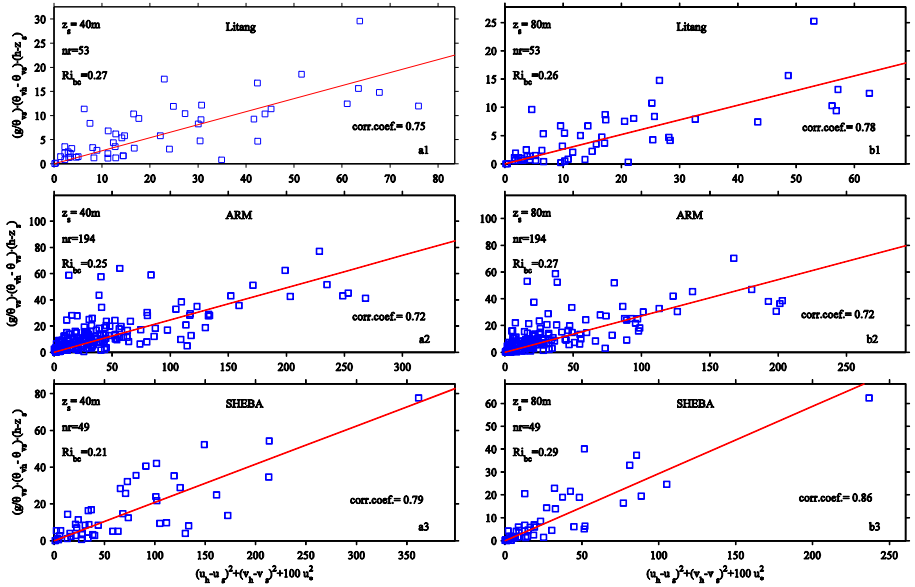

Figure 5. Comparisons of the numerator and denominator from Eq. (3) for the Type II SBL, with z_s at 40 m (left) and 80 m (right). The PBLHs determined by the LLJ method for Litang, ARM Shouxian, and SHEBA data are used. nr refers to the effective sample number. The red solid lines are the best linear fittings of the data from different sites and their slopes represent the values of the critical bulk Richardson number Ri_{bc}.

GMDD
7, 4045–4079, 2014

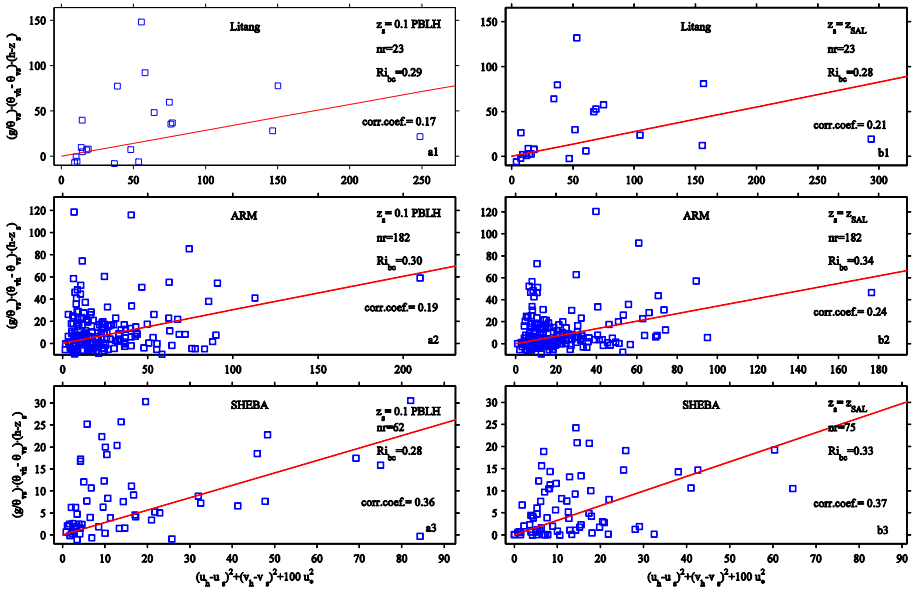

Figure 6. Comparisons of the numerator and denominator from Eq. (3) for the UBL, with z_s at 0.1 PBLH (left) and z_{SAL} (right). The PBLHs determined by the modified parcel method for Litang, ARM Shouxian, and SHEBA data are used. nr refers to the effective sample number. The red solid lines are the best linear fittings of the data from different sites and their slopes represent the values of the critical bulk Richardson number Ri_{bc}.

GMDD
7, 4045–4079, 2014

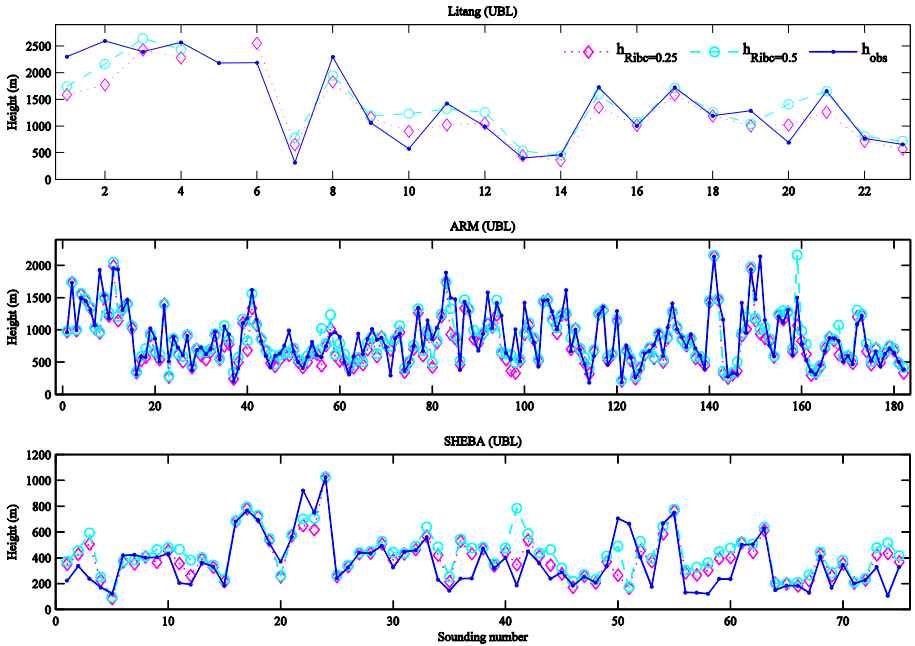

Figure 7. Comparisons of the UBL height in different sites determined by the Ri_b method with Ri_{bc} = 0.25 (diamond) and 0.5 (circle) to that determined by the modified parcel method (point).

GMDD
7, 4045–4079, 2014

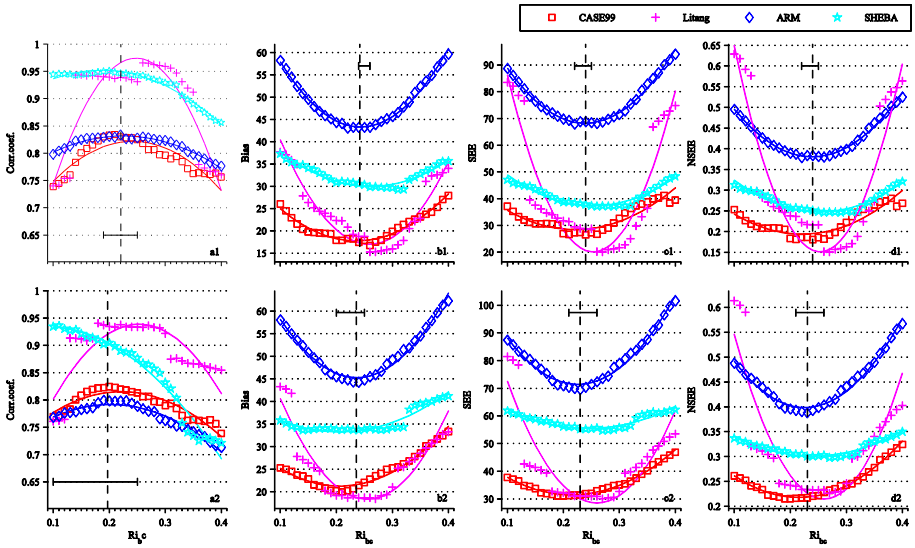

Figure 8. Comparison between PBLH estimated using the Bulk Richardson number method with z_s at 40 m (upper panels) and 80 m (lower panels) and PBLH estimated using the Tur method (for CASES99) and using the PTG method (for the other three sites) for the Type I SBL. The correlation coefficient **(a)**, bias **(b)**, standard error **(c)**, and normalized standard error **(d)** are shown. The sounding data are taken from Litang (plus sign), CASES99 (square), ARM Shouxian (diamond), and SHEBA (pentacle). The curved linesare obtained by quadratic curve-fitting, the black vertical dashed lines indicate a representative Ri_{bc} for all four sites, and the error bars indicate the range of Ri_{bc} across the four sites.

GMDD
7, 4045–4079, 2014

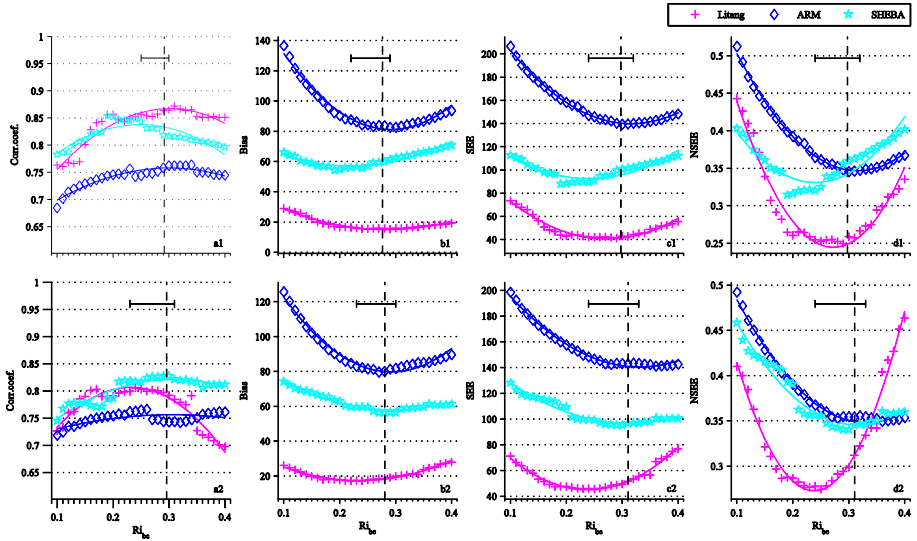

Figure 9. Comparison between PBLH estimated using the Bulk Richardson number method with z_s at 40 m (upper panels) and 80 m (lower panels) and PBLH estimated using the LLJ methodfor the Type II SBL. The correlation coefficient **(a)**, bias **(b)**, standard error **(c)**, and normalized standard error **(d)** are shown. The sounding data are taken from Litang (plus sign), ARM Shouxian (diamond), and SHEBA (pentacle). The curved linesare obtained by quadratic curve-fitting, the black vertical dashed lines indicate a representative Ri_{bc} for all three sites, and the error bars indicate the range of Ri_{bc} across the three sites.

GMDD
7, 4045–4079, 2014

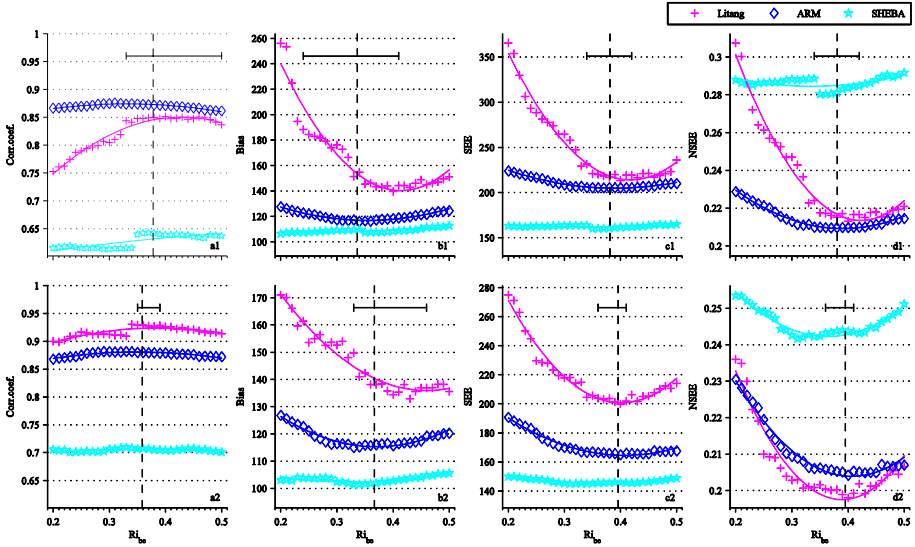

Figure 10. Comparison between PBLH estimated using the Bulk Richardson number method with z_s at 0.1 PBLH (upper panels) and z_{SAL} (lower panels) and PBLH estimated using the modified parcel methodfor the UBL. The correlation coefficient **(a)**, bias **(b)**, standard error **(c)**, and normalized standard error **(d)** are shown. The sounding data are taken from Litang (plus sign), ARM Shouxian (diamond), and SHEBA (pentacle). The curved linesare obtained by quadratic curve-fitting, the black vertical dashed lines indicate a representative Ri_{bc} for all three sites, and the error bars indicate the range of Ri_{bc} across the three sites.

GMDD
7, 4045–4079, 2014

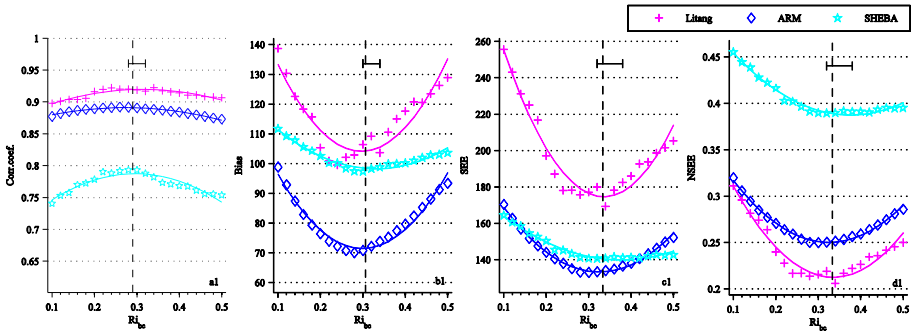

Figure 11. Comparison between PBLH estimated using the Bulk Richardson number method with z_s = 40 m for the Type I SBL, 80 m for the Type II SBL, z_{sal} for the UBL and PBLH estimated using the PTG, LLJ, and modified parcel method. The correlation coefficient **(a)**, bias **(b)**, standard error **(c)**, and normalized standard error **(d)** are shown. The sounding data are taken from Litang (plus sign), ARM Shouxian (diamond), and SHEBA (pentacle). The curved linesare obtained by quadratic curve-fitting, the black vertical dashed lines indicate a representative Ri_{bc} for all three sites, and the error bars indicate the range of Ri_{bc} across the three sites.

GMDD
7, 4045–4079, 2014

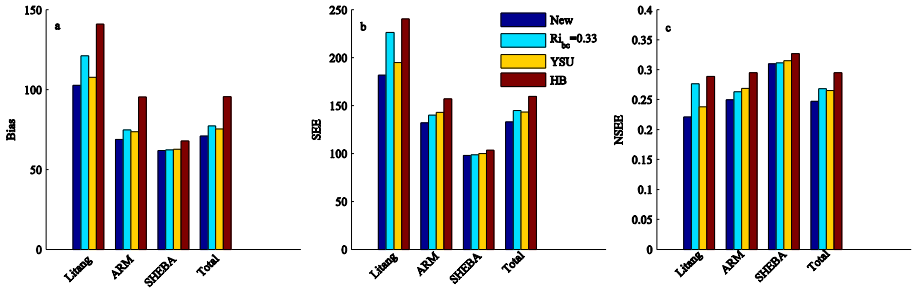

Figure 12. Error analysis of the PBLH determined by the Ri_b method with a single $Ri_{bc} = 0.33$ for all PBL conditions, the YSU scheme ($Ri_{bc} = 0.25$), the HB scheme ($Ri_{bc} = 0.5$), and the new scheme ($Ri_{bc} = 0.24$, 0.31, and 0.39 for the Type I SBL, Type II SBL, and UBL, respectively): **(a)** bias; **(b)** standard error; **(c)** normalized standard error.

GMDD
7, 4045–4079, 2014